Article

Not peer-reviewed version

# Thermal Surface Properties, London Dispersive and Polar Sur-face Energy of Graphene and Carbon Materials by Inverse Gas Chromatography at Infinite Dilution

Tayssir Hamieh *

Posted Date: 24 May 2024

doi: 10.20944/preprints202405.1631.v1

Keywords: London dispersion equation; Hamieh thermal model; Thermal conductivity; London dispersive and polar surface energy; Lewis's acid–base constants; coupling amphoteric constant; average separation distance between particles; acid and base surface energy

 doi:10.20944/preprints202405.1631.v1



*Article*

# Thermal Surface Properties, London Dispersive and Polar Surface Energy of Graphene and Carbon Materials by Inverse Gas Chromatography at Infinite Dilution

**Tayssir Hamieh** [1,2]

[1] Faculty of Science and Engineering, Maastricht University, P.O. Box 616, 6200 MD Maastricht, The Netherlands; t.hamieh@maastrichtuniversity.nl
[2] Laboratory of Materials, Catalysis, Environment and Analytical Methods (MCEMA), Faculty of Sciences, Lebanese University, Beirut P.O. Box 6573/14, Lebanon

**Abstract:** The thermal surface properties of graphenes and carbon materials are of crucial importance in chemistry of materials, chemical engineering, and many industrial processes. (1) Background: The determination of these surface properties is carried out using inverse gas chromatography at infinite dilution which leads to the retention volume of organic solvents adsorbed on solid surfaces. This experimental and fundamental parameter actually reflects the surface thermodynamic interactions between injected probes and solid substrates. (2) Methods: The London dispersion equation and the Hamieh thermal model were used to quantify the London dispersive and polar surface energy of graphenes and carbon fibers as well their Lewis acid-base constants by introducing the coupling amphoteric constant of materials. (3) Results: The London dispersive and polar acid-base surface energies, the free energy of adsorption, the polar enthalpy and entropy, and the Lewis acid-base constants of graphenes and carbon materials were determined. (4) Conclusions: it was showed that graphene exhibited the highest values of London dispersive surface energy, polar surface energy, and Lewis's acid-base constants. These highest characteristics of graphene justify its great potentiality and uses in many industrial applications.

**Keywords:** London dispersion equation; Hamieh thermal model; thermal conductivity; London dispersive and polar surface energy; Lewis's acid–base constants; coupling amphoteric constant; average separation distance between particles; acid and base surface energy

## 1. Introduction

The determination of the thermal surface properties of materials and their dispersive, polar and Lewis's acid-base energies, is of great interest in many industrial applications and fundamental sciences. These various surface properties are directly correlated to the interactions between materials and adsorbents and ply an important role in several scientific disciplines such as adhesion, adsorption, diffusion, evaporation, condensation, coatings, friction, conduction, chemical engineering, catalysis, and electronics. The behavior of materials strongly depends on their surface properties and the dependency of such properties from the temperature. Indeed, the temperature exerts an important effect on the interactions between particles or molecules, their London dispersive and polar surface energies, and their Lewis acid-base properties. The variations, against the temperature, of adhesive, two-dimensional state, and surface properties of materials such as oxides, polymers, composites, graphite, and carbon, are generally used in many industrial processes.

Carbon materials forming a large variety of allotropes, present very interesting physicochemical and mechanical properties, very used to replace conventional metals for various applications by decreasing the weight of products, and they are very famous for their thermal properties. Indeed, the

 doi:10.20944/preprints202405.1631.v1



thermal conductivity of carbon allotropes vary from 0.01 W $m^{-1}$ $K^{-1}$ in amorphous carbon to more than 2,000 W $m^{-1}$ $K^{-1}$ in diamond or graphene [1].

The Graphene exfoliation [2] led to the highest electrical conduction and allowed to investigate the heat transport in 2D crystals [3]. Experimental measurements of the thermal conductivity of graphene were carried out by several research works [4–9]. The availability of high-quality few-layer graphene (FLG) led to experimental observations of the evolution of thermal properties as the system dimensionality changes from 2D to 3D [6]. Several authors studied the thermal properties of graphene and showed its higher thermal conductivity [9–13].

Paz et al. [14] investigated the effect of an epitaxially-grown graphene layer replacing the metallic contact over the active region in Silicon carbide diodes as radiation detectors. Indeed, the surface properties of graphene usually play an important role in the practical application of graphene-based materials, especially, in the nano-composites, nano-coating and electrical nanodevices [15].

The effect of high temperature on structure of graphene and the changes in its morphology were studied by Amanda et al. [16]. The synthesis of graphene oxide (GO) by electrochemical oxidation of graphite and the reduction of electrochemically-derived GO (EGO) were carried out by Xiong et al. [17] and easily transformed into high-crystalline graphene membranes. Graphene and graphene oxide (GO) were used to improve the properties of traditional cement-based building materials [18].

Kumuda et al. [19] explored several synthesis methods, structural distinctions, and a range of analytical techniques employed to compare properties among graphite, graphene oxide, and reduced graphene oxide (rGO). Some surface properties such as the surface energy of graphene and graphene oxide were studied by Wang et al. [20] that obtained 46.7 and 62.1 mJ/$m^2$, respectively, while natural graphite flake presented a surface free energy of 54.8 mJ/$m^2$ at room temperature.

The use of IGC technique at infinite dilution to determine the surface properties of graphene oxide (GO) and graphene (rGO) was carried out for the first time by Dai et al. [21]. However, the results obtained by these authors were based on the hypothesis which considered the surface area and the London dispersive surface energy of the organic molecules as constant parameters. This was failed by several research works [22–26] proving an important variation of the above parameters as a function of the temperature. Lee et al. [27] also determined the London dispersive and polar components, and the Lewis acid-base properties of the surface free energy of graphene materials using IGC technique at an infinite dilution at room temperature. The same previous critiques can be formulated on the results obtained by Lee et al. [27] that limited their studies only to the room temperature.

The lack of information and the different gaps encountered in this research area guided the objective of our study for an accurate determination of the surface properties of graphene and carbon materials which are very required to obtain a real guidance for the design and manufacturing of graphene-based biomaterials, medical instruments, structural composites, electronics, and renewable energy devices [20]. The present work is then devoted to the determination of thermal surface properties, the London dispersive and polar acid-base surface energies, and the Lewis's acid-base parameters of graphene and carbon materials as a function of the temperature by using IGC technique [28–76] at infinite dilution and applying our new approach based on the Hamieh thermal model [22–26].

## 2. Results

### *2.1. London Dispersive Surface Energy of Solid Materials*

The experimental results of the net retention volume $V_n$ of organic molecules adsorbed on the various solid surfaces as a function of the temperature $T$ allowed giving the variations $RTlnV_n(T)$ against the temperature for n-alkanes and polar molecules (Figure S1). An important variation was reported in the behavior of $RTlnV_n$ of organic molecules adsorbed on the different solid substrates. The highest values were obtained in the case of graphene followed by those of reduced graphene oxide. Whereas, the lowest values of $RTlnV_n$ were obtained with the untreated carbon fibers. Figure S1 also showed that the values obtained with graphene were 2.5 times grated than those of the

 doi:10.20944/preprints202405.1631.v1



untreated carbon fibers, thus proving a priori a higher chemical activity of graphene relative to that of carbon materials.

The obtained results of $RTlnV_n$ and the application of the Hamieh thermal model which gave the expressions of the surface area $a(T)$ and the dispersive surface energy $\gamma_l^d(T)$ of organic molecules as a function of the temperature $T$ [22–26], led to the representation of $RTlnV_n$ as a function of $2\mathcal{N}a(T)\left(\gamma_l^d\right)^{1/2}$ in Figure 1 for graphene and carbon materials.

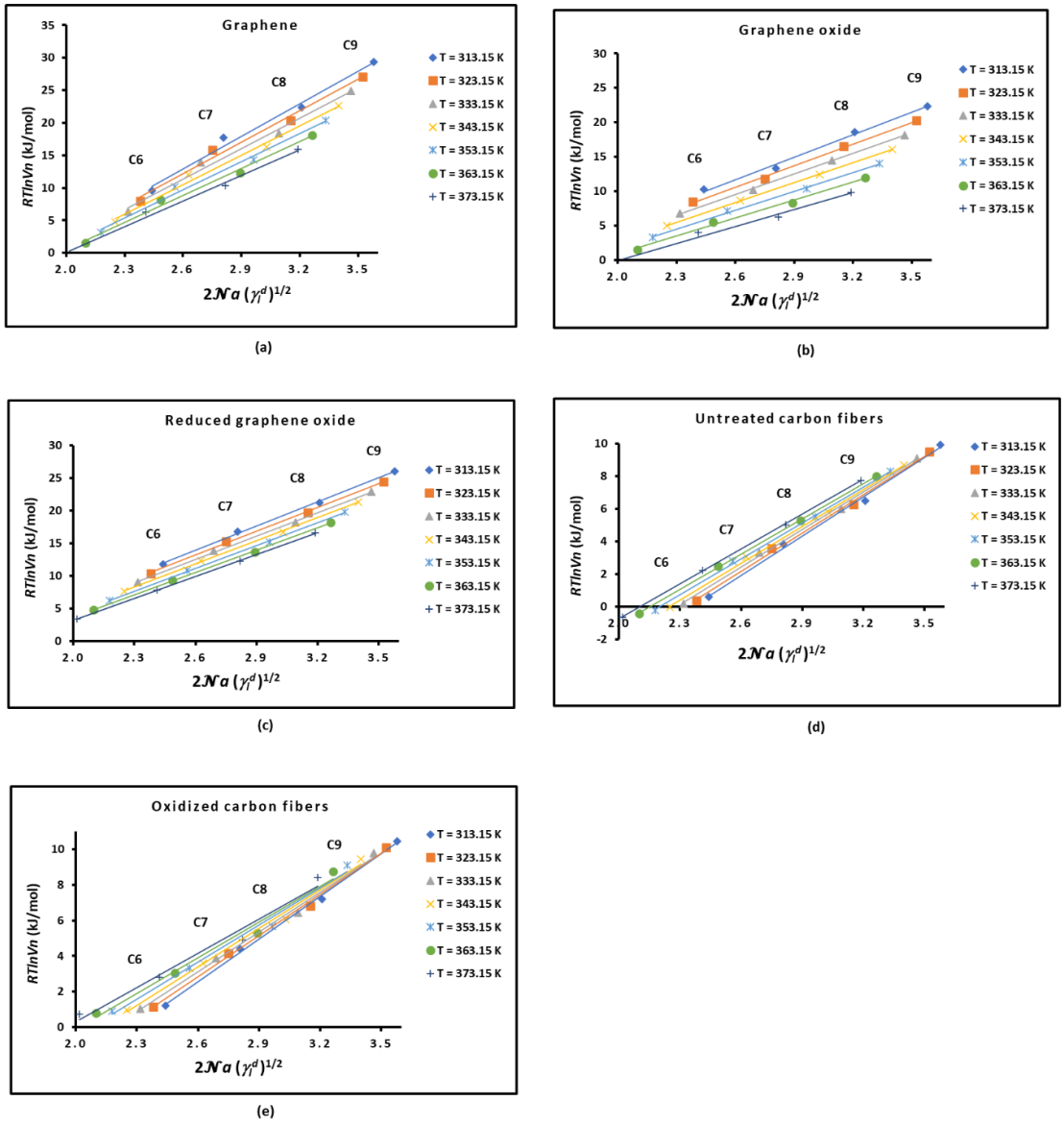


**Figure 1.** Variations of $RTlnV_n(T)$ as a function of $2\mathcal{N}a(T)\left(\gamma_l^d\right)^{1/2}$ of n-alkanes (from n-hexane (C6) to n-nonane (C9)) adsorbed on the different solid materials at different temperatures. (a) Graphene, (b) Graphene oxide, (c) reduced graphene oxide, (d) Untreated carbon fibers, and (e) Oxidized carbon fibers.

The slope of the straight-line of $RTlnV_n(T) = f\left[2\mathcal{N}a(T)\left(\gamma_l^d\right)^{1/2}\right]$ obtained in Figure 1 for the different solid surfaces and at various temperatures allowed to an accurate determination of the London dispersive surface energy of $\gamma_s^d(T)$ of the various solids by using the Hamieh thermal model. The obtained results were plotted in Figure 2.

 doi:10.20944/preprints202405.1631.v1



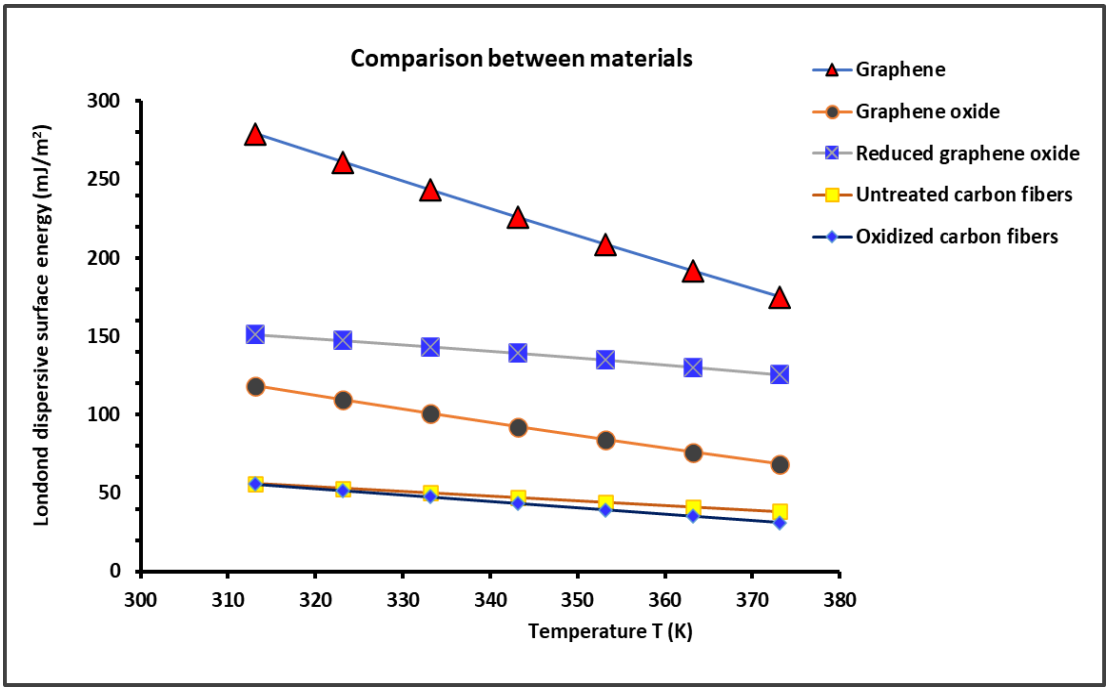


**Figure 2.** Evolution of the London dispersive surface energy of graphene and carbon materials as a function of the temperature.

Figure 2 showed that the graphene exhibited the highest $\gamma_s^d(T)$for all temperatures followed by the reduced graphene oxide, while the lowest $\gamma_s^d(T)$ was obtained in the case of the oxidized carbon fibers. The results showed a slight variation of $\gamma_s^d(T)$ between the untreated and oxidized carbon fibers. However, the oxidation of graphene considerably reduced the value of $\gamma_s^d(T)$, about 50% at 40°C. This highlighted the strong effect of the chemical structure on the value of the London dispersive surface energy of materials. Table 1 showed the difference between the various materials in the values of the London dispersive surface entropy $\varepsilon_s^d$, the extrapolated London dispersive surface energy at 0K $\gamma_s^d(T = 0\text{K})$, and the temperature maximum $T_{Max}$.

**Table 1.** Equations $\gamma_s^d(T)$ of graphene, graphene oxide, reduced graphene oxide, carbon fibers, untreated and oxidized, with the London dispersive surface entropy $\varepsilon_s^d$, the extrapolated London dispersive surface energy at 0K $\gamma_s^d(T = 0K)$, and the temperature maximum $T_{Max}$.

| **Solid material** | $\boldsymbol{\gamma_s^d(T)}$ **(mJ/m²)** | $\boldsymbol{\varepsilon_s^d = d\gamma_s^d/dT}$ **(mJ m⁻² K⁻¹)** | $\boldsymbol{\gamma_s^d(T = 0K)}$ **(mJ/m²)** | $\boldsymbol{T_{Max}}$ **(K)** |
|---|---|---|---|---|
| Graphene | $\gamma_s^d(T)$ = -1.736T + 822.22 | -1.736 | 822.22 | 473.5 |
| Graphene oxide | $\gamma_s^d(T)$ = -0.832T + 377.98 | -0.832 | 377.98 | 454.6 |
| Reduced graphene oxide | $\gamma_s^d(T)$ = -0.424T + 284.29 | -0.424 | 284.29 | 670.5 |
| Untreated carbon fibers | $\gamma_s^d(T)$ = -0.295T + 148.22 | -0.295 | 148.22 | 502.8 |
| Oxidized carbon fibers | $\gamma_s^d(T)$ = -0.409T + 183.60 | -0.409 | 183.60 | 449.4 |

The comparison between the results given in Table 1 and those of literature [15,21,27,77–80] showed large differences in the values of the London dispersive surface energy. Dai et al. [21] in 2014 obtained for GO and rGO the respective values of $\gamma_s^d$: 28.5 mJ/m² and 98.3 mJ/m² at 313.15K. However, the same authors [77] in 2015 gave the following values: $\gamma_s^d$: 78.9 mJ/m² and 106.8 mJ/m² respectively for the graphene oxide and reduced graphene oxide. Whereas, Lee et al. [27] obtained the results given in Table 2 and compared to our results.

 doi:10.20944/preprints202405.1631.v1



**Table 2.** Comparison between the values alues of the London dispersive surface energy $\gamma_s^d$ of graphene oxide and reduced graphene oxide at 313.15K, obtained in this work compared to those of literature.

| Solid material | $\gamma_s^d(T)$ (mJ/m²) Lee et al. [27] | $\gamma_s^d(313.15K)$ (mJ/m²) Dai et al. [21] | $\gamma_s^d(313.15K)$ (mJ/m²) Dai et al. [77] | $\gamma_s^d(313.15K)$ (mJ/m²) This work |
|---|---|---|---|---|
| Graphene oxide | 110 | 28.5 | 78.9 | 118.2 |
| Reduced graphene oxide | 125 | 98.3 | 106.8 | 151.0 |

Table 2. showed that the deviation between the results of Dai et al. [21,77] with those obtained by Hamieh thermal model varies from 33% to 76% for GO and from 29% to 35% for rGO. Whereas, the deviation with the results obtained by Lee et al. [27] is 7% for GO and 17% for rGO.

Lee et al. [27] gave the following variations of $\gamma_s^d(T)$ as a function of temperature in the interval [300K; 400K]: for graphene oxide: $\gamma_s^d(T)$ = -0.540T + 279.0 and for reduced graphene oxide: $\gamma_s^d(T)$ = -0.279T + 212.02. These results also showed an important variation in the values of the London dispersive surface entropy $\varepsilon_s^d$ and the extrapolated London dispersive surface energy $\gamma_s^d(T = 0\text{K})$ with those obtained by the hamieh thermal model shown in Table 1. This large deviation between the results of literature and those of the thermal model is certainly due to the fact that the effect of the temperature on the surface area of the organic molecules was neglected during the calculation of the London dispersive surface energy of materials.

On the other hand, the previous results shown in Figure 2 and Table 1 can be correlated to the thermal conductivity $K$ of graphene and carbon materials. Figure 3 gave the variations of the thermal conductivity as a function of temperature by using the data of literature [6,9–12,81–84]. In the studied temperature interval [300K; 400K, it was observed that the thermal conductivity $K$ decreases when the temperature increases for the graphene, the graphite and the carbon fiber. The results in Figure 3 highlighted the highest thermal conductivity of graphene which also exhibited the highest London dispersive surface energy.

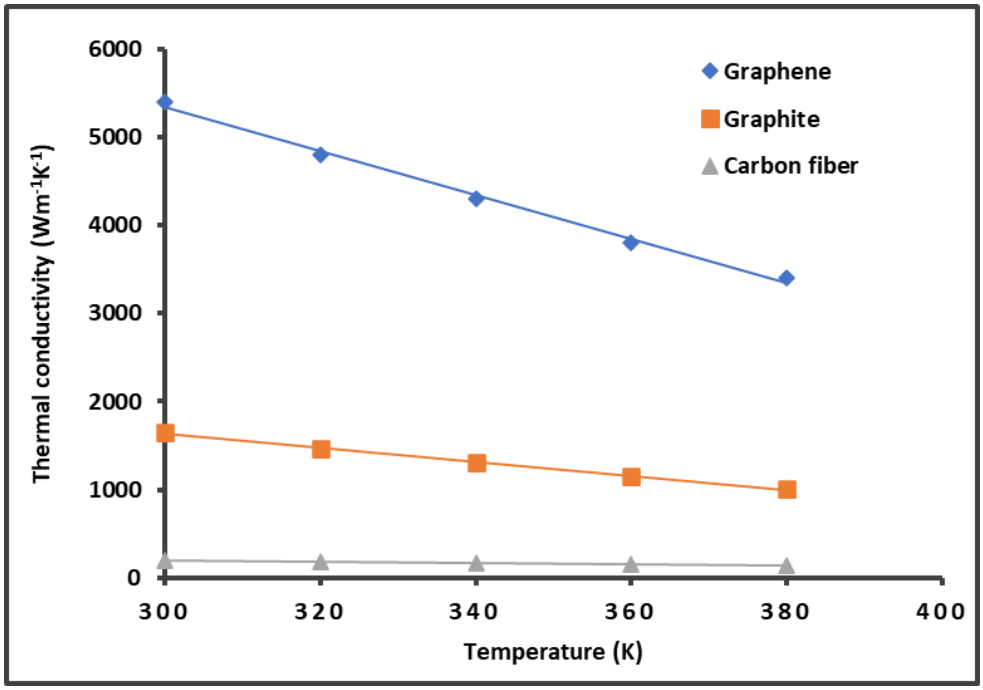


**Figure 3.** Variations of the thermal conductivity $K$ of graphene and carbon materials as a function of the temperature.

 doi:10.20944/preprints202405.1631.v1



This result led us to see if there is a direct correlation between the thermal conductivity of material and its London dispersive surface energy, not only for graphene and carbon materials but also for other metallic oxide such as alumina, magnesium oxide and zinc oxide. The values of the thermal conductivity were taken from the works of Hofmeister [85] and Wu et al. [86], whereas, those of the London dispersive energy were obtained in previous studies [67,74,75].

The variations of London dispersive surface energy $\gamma_s^d(T)$ and the thermal conductivity $K(T)$ of some solid materials such as alumina, MgO, ZnO, graphene, graphite, and carbon fiber as a function of the temperature were plotted in Figure 4.

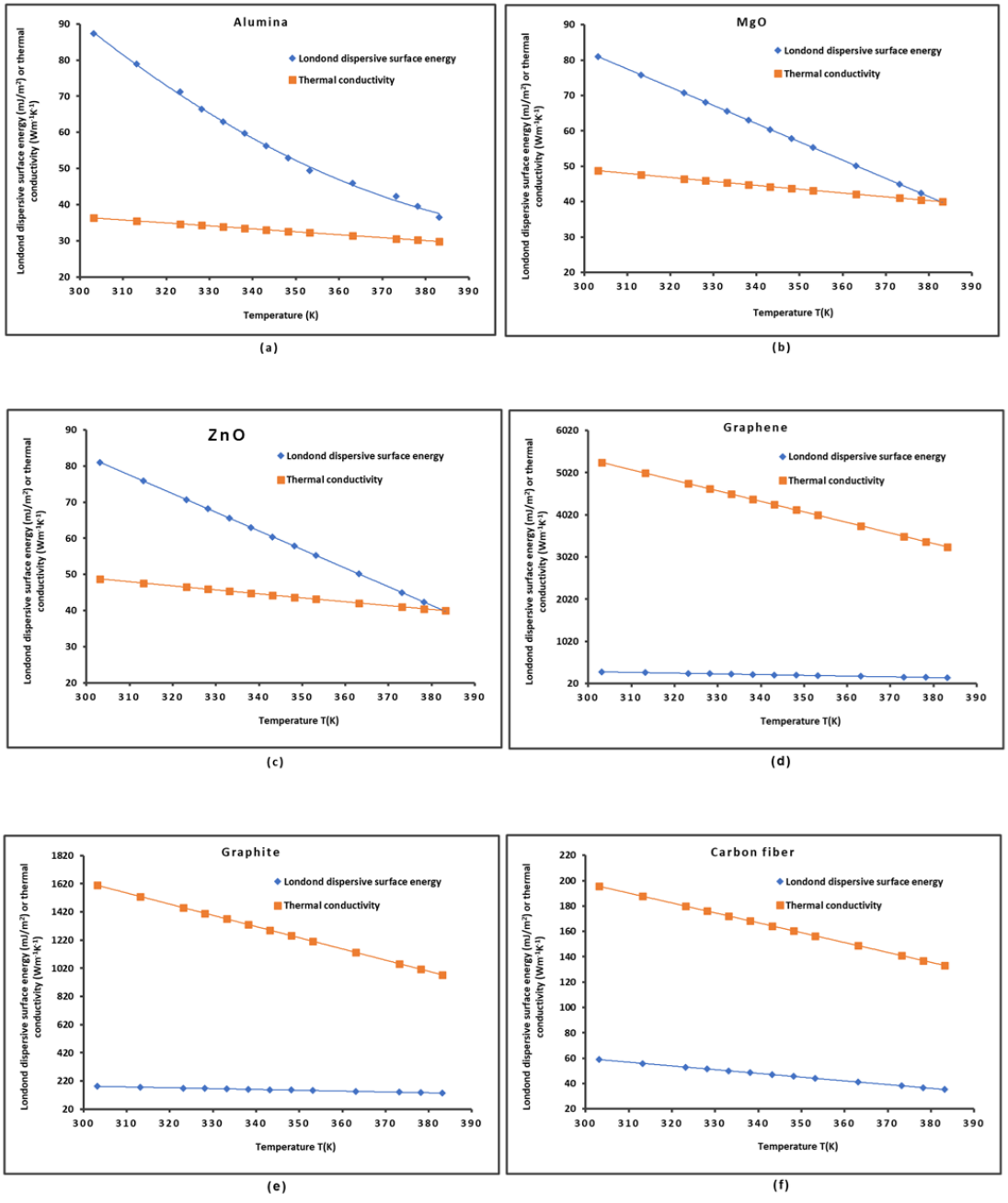


**Figure 4.** Evolution of the London dispersive surface energy $\gamma_s^d(T)$ and the thermal conductivity $K(T)$ of alumina (a), MgO (b), ZnO (c), graphene (d), graphite (e), and carbon fiber (f) as a function of the temperature.

The curves in Figure 4 all present a decrease of $\gamma_s^d(T)$ and $K(T)$ when the temperature increases. The functions $\gamma_s^d(T)$ and $K(T)$ are perfectly fitted by parabolic or linear curves with linear

 doi:10.20944/preprints202405.1631.v1



regression coefficients equal to 1.000. The highest values of $\gamma_s^d(T)$ and $K(T)$ were obtained for graphene showing the superiority of this material relative to the other materials for several applications.

The variations of the thermal conductivity $K(T)$ as a function of the London dispersive surface energy $\gamma_s^d(T)$ of different solid materials plotted in Figure 5 also showed parabolic or linear curves. The perfect linearity was assured for MgO, graphene, carbon fiber, and graphite, whereas perfect parabolic functions were obtained in the case of ZnO and alumina (Figure 5a) with linear regression coefficients equal to $R^2 = 1.000$.

Preprints.org (www.preprints.org) | NOT PEER-REVIEWED | Posted: 24 May 2024 doi:10.20944/preprints202405.1631.v1



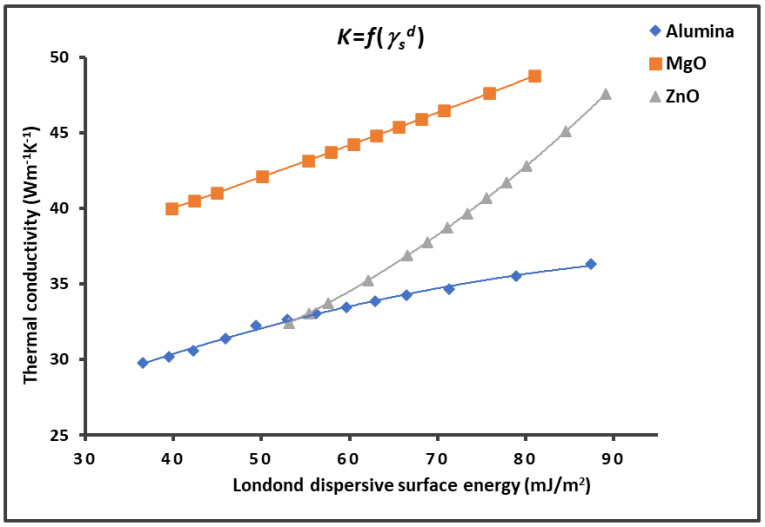


(a)

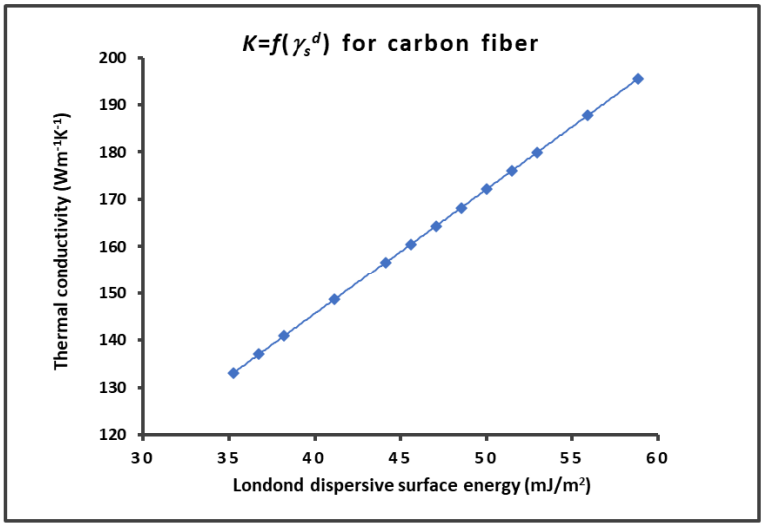


(b)

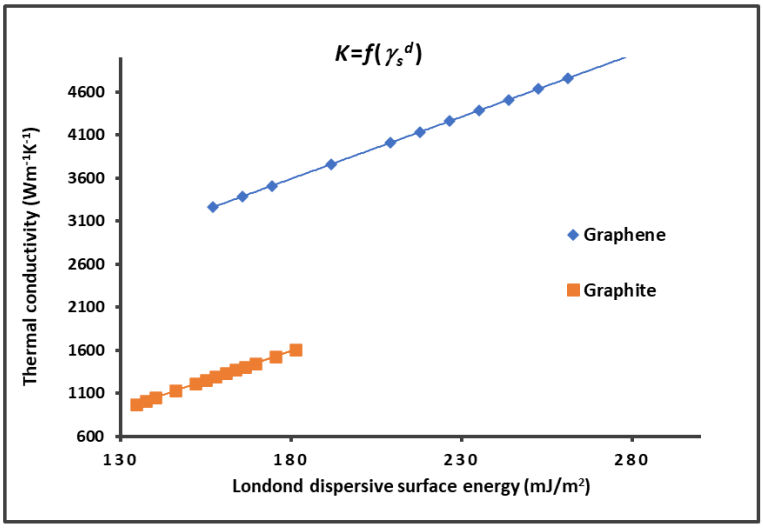


(c)

 doi:10.20944/preprints202405.1631.v1



**Figure 5.** Variations of the thermal conductivity $K(T)$ of alumina, MgO, and ZnO (a), carbon fiber (b), and graphene and graphite (c) as a function of the London dispersive surface energy $\gamma_s^d(T)$.

The results allowed to give in Table 3 the various equations obtained for the different solid materials.

**Table 3.** Equations of the thermal conductivity of materials as a function of the London dispersive surface energy $K = f(\gamma_s^d)$.

| **Material** | **Equation $K = f(\gamma_s^d)$** |
|---|---|
| MgO | $K$ = 0.2124 $\gamma_s^d$ + 31.47 |
| Graphene | $K$ = 14.398 $\gamma_s^d$ + 1002 |
| Graphite | $K$ = 13.613 $\gamma_s^d$ + 856.09 |
| Carbon fiber | $K$ = 2.646 $\gamma_s^d$ + 39.83 |
| Alumina | $K$ = -0.0012 $(\gamma_s^d)^2$ + 0.281 $\gamma_s^d$ + 21.123 |
| ZnO | $K$ = 0.004 $(\gamma_s^d)^2$ - 0.142 $\gamma_s^d$ + 28.794 |

Table 3 and the curves of Figures 5 clearly showed the important correlation between the thermal conductivity $K(T)$ of materials and of the London dispersive surface energy $\gamma_s^d(T)$. Knowing one of these two parameters at certain temperature, one can deduce the other. It can be concluded that the higher the London dispersive surface energy, the higher the thermal conductivity.

*2.2. Lewis's Acid-Base Properties of Solid Materials*

Our new approach based on the London interaction energy was used to determine the free specific energy $-\Delta G_a^p(T)$ of interaction between the solid substrates and the different chosen polar organic solvents. The results were given in Table S1 for graphene, graphene oxide, reduced graphene oxide, untreated carbon fibers, and oxidized carbon fibers. It was observed that the graphene exhibited the highest polar free energy for all polar molecules with greater values with basic solvents reflecting its highest acidic character.

The comparison between the different solid materials was elucidated in Figure 6. It can be deduced that the interaction energy is the highest with graphene, respectively followed by graphene oxide and reduced graphene oxide which presents the lowest polar energy between the three graphenes. Figure 6 also showed that the reduced graphene oxide presents polar free energy values very close to those of the untreated carbon fibers, whereas, similar values were obtained for graphene oxide and oxidized carbon fibers in the case of acid solvent.

Preprints.org (www.preprints.org) | NOT PEER-REVIEWED | Posted: 24 May 2024 doi:10.20944/preprints202405.1631.v1



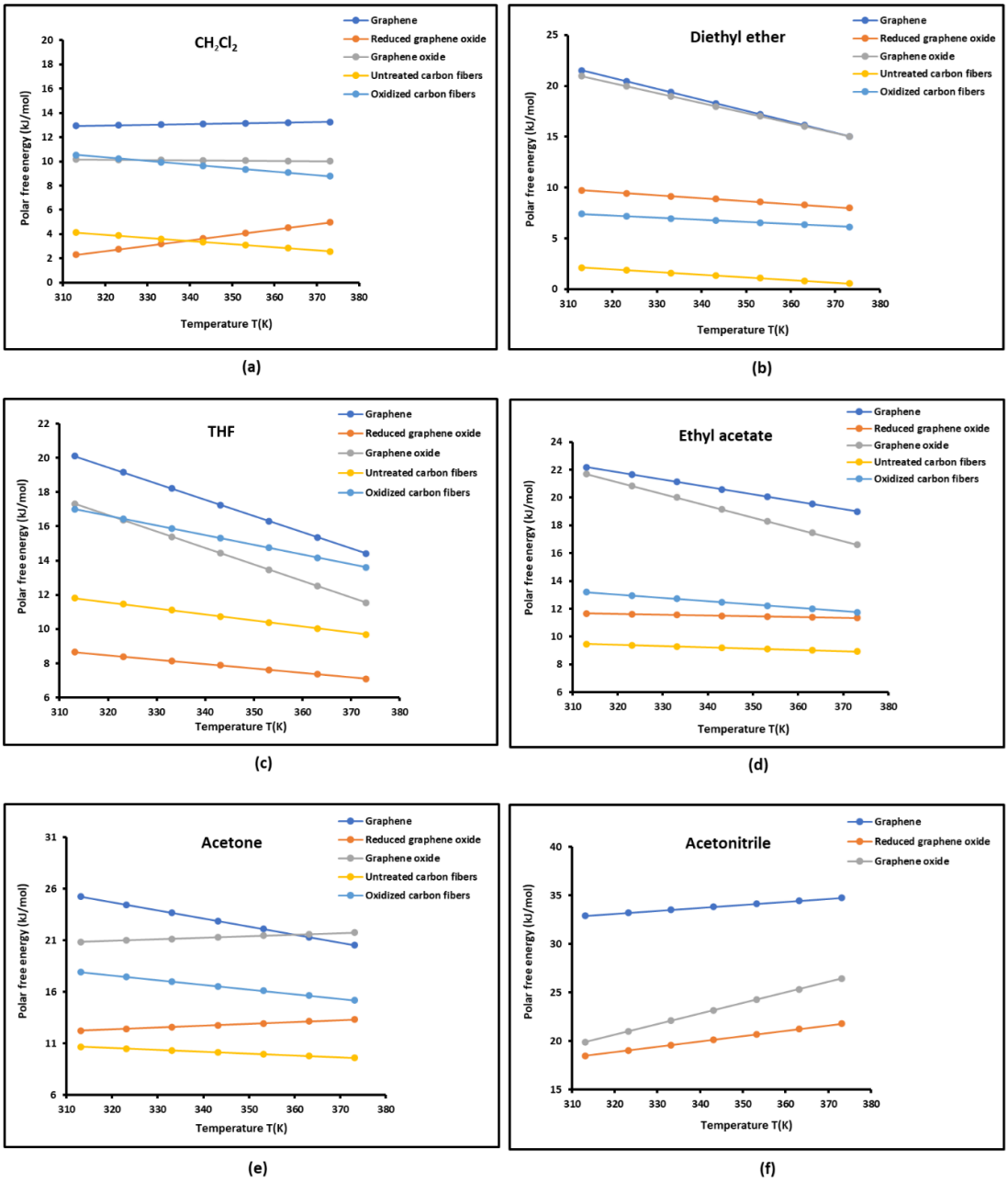


**Figure 6.** Variations of the polar free interaction energy $-\Delta G_a^p(T)$ of the various polar solvents adsorbed on the different graphene and carbon materials as a function of temperature. (a): Dichloromethane, (b): Diethyl ether, (c): THF, (d): Ethyl acetate, (e): acetone, and (f): acetonitrile.

This led concluding that the oxidation of carbon materials gives similar interaction energy certainly due to the presence of identical surface groups such as carboxylate, hydroxyl, and epoxy. However, the gap between graphenes and carbon fibers increases in the case of basic or amphoteric polar molecules. This results from the difference in the acidic behavior of the different materials.

To quantify the acid-base behavior of different solid materials, it was necessary to determine the values of polar enthalpy $(-\Delta H_a^p)$ and entropy $(-\Delta S_a^p)$ of adsorbed polar molecules, using the variations of $-\Delta G_a^p(T)$ against the temperature. The results were given in Tables S2 and S3. They also showed the highest polar enthalpy of graphene in interaction with the basic and amphoteric solvents again proving the highest Lewis acidity of graphene relative to other graphenes and carbon materials.

 doi:10.20944/preprints202405.1631.v1



The representation of $\left(\frac{-\Delta H_a^p}{AN'}\right)$ and $\left(\frac{-\Delta S_a^p}{AN'}\right)$ as a function of $\left(\frac{DN'}{AN'}\right)$ of the different polar solvents adsorbed on the solid surfaces led to the values of the Lewis enthalpic $K_A$ and $K_D$ and entropic $\omega_A$ and $\omega_D$ acid–base constants of graphenes and carbon fibers. These acid-base values were given in Table 4. However, negative values were obtained for the Lewis acid-base constants were obtained in certain solid surfaces such as graphene oxide, reduced graphene oxide, and oxidized carbon fibers. Whereas, the accepted values for graphene and untreated carbon fibers showed the highest acidity of graphene with a ratio $K_A/K_D$ = 2.4 and highest basicity of untreated carbon fibers with a ratio $K_A/K_D$ = 0.7.

**Table 4.** Values of the acid–base constants $K_A$, $K_D$, $\omega_A$, $\omega_D$ and linear regression coefficients $R^2$ of graphenes and carbon fibers with the corresponding acid–base ratios.

| Material | $K_D$ | $K_A$ | $K_D/K_A$ | $R^2$ | $10^{-3}\omega_A$ | $10^{-3}\omega_D$ | $\omega_D/\omega_A$ | $R^2$ |
|---|---|---|---|---|---|---|---|---|
| Graphene | 0.253 | 0.593 | 0.426 | 0.9906 | -1.346 | 1.187 | -1.134 | 0.9563 |
| Graphene oxide | -0.551 | 0.223 | -2.471 | 0.9833 | -3.305 | 0.416 | -7.951 | 0.9412 |
| Reduced graphene oxide | -0.721 | 0.601 | -1.200 | 0.9608 | -1.800 | 1.232 | -1.461 | 0.9421 |
| Untreated carbon fibers | 0.345 | 0.235 | 1.468 | 0.8465 | 0.927 | 0.348 | 2.663 | 0.7631 |
| Oxidized carbon fibers | -0.010 | 0.381 | -0.025 | 0.9120 | -0.613 | 0.630 | -0.973 | 0.9002 |

Nevertheless, the negative values of the acid-base constants indicates that the empirical relation $-\Delta H^p = DN \times K_A + AN \times K_D$ used to calculate these constants should be corrected. In previous paper [59], a new relation was proposed consisting in taking into account the amphoteric effect by adding a new coupling acid-base constant $K_{CC}$ which corrects this gap: $-\Delta H^p = K_A \times DN + K_D \times AN - K_{CC} \times AN \times DN$. The resolution of such linear system was developed in several previous works [26,59,64,75]. The results obtained by using this correction were included in Table 5.

**Table 5.** Corrected values of the acid–base constants $K_A$, $K_D$, and new amphoteric constant $K$ of graphenes and carbon fibers with the corresponding acid–base ratios $K_D/K_A$.

| Material | $K_D$ | $K_A$ | $K_{CC}$ | $K_D/K_A$ |
|---|---|---|---|---|
| Graphene (G) | 0.278 | 0.594 | $5.7\times10^{-4}$ | 0.468 |
| Graphene oxide (GO) | 0.227 | 0.069 | $-7.9\times10^{-3}$ | 3.306 |
| Reduced graphene oxide (rGO) | 0.217 | 0.631 | $2.1\times10^{-2}$ | 0.344 |
| Untreated carbon fibers (UCF) | 1.587 | 0.325 | $4.4\times10^{-2}$ | 4.883 |
| Oxidized carbon fibers (OCF) | 1.190 | 0.468 | $4.2\times10^{-2}$ | 2.543 |

Nevertheless, the negative values of the acid-base constants indicates that the empirical relation $-\Delta H^p = DN \times K_A + AN \times K_D$ used to calculate these constants should be corrected. In previous paper [59], a new relation was proposed consisting in taking into account the amphoteric effect by adding a new coupling acid-base constant $K_{CC}$ which corrects this gap: $-\Delta H^p = K_A \times DN + K_D \times AN - K_{CC} \times AN \times DN$. The resolution of such linear system was developed in several previous works [26,59,64,75]. The results obtained by using this correction were included in Table 5.

The corrected Lewis's acid-base constants of the different solid materials led to positive values of $K_A$ and $K_D$ with a new coupling constant $K_{CC}$. The results in Table 5 allowed us giving the classification of the above materials in increasing order of their Lewis basicity as follows:

$$rGO \leq GO < G < OCF < UCF$$

This implied that the untreated carbon fiber exhibited the highest basic character, whereas, the lowest basicity was obtained with the reduced graphene oxide, while graphene had a slightly higher basic constant between the three graphenes which admitted comparable basicity.

The comparison between the Lewis acidity strengths was given in increasing order of acid character as follows:

 doi:10.20944/preprints202405.1631.v1



$$GO < UCF < OCF < G \leq rGO$$

Indeed, the large difference between the graphene behaviors was due to the important variation in acidic interaction force of these materials. Graphene and reduced graphene oxide exhibited the highest acidity, whereas, graphene oxide showed the lowest acid character. On the other hand, Table 5 highlighted a higher ratio $K_D/K_A$ compared to other graphenes certainly due to the presence of several surface basic groups such carboxylate, hydroxyl, and epoxy.

In conclusion, it was proved that graphene and reduced graphene oxide more acidic than basic (in Lewis terms), whereas, graphene and carbon fibers exhibited higher basic character. These results are in perfect agreement with the surface nature of the various materials. The oxidation of graphene increased the basic character of the material, while the reduction of graphene oxide increased the acid interaction force. The natural carbon fiber highlighted the highest basicity (about 5 times more basic than acidic).

The results obtained by Dai et al. [21] and Lee et al. [27] showed rather a basic character for reduced graphene oxide at contrary of the results of our present work. In fact, the values of Lewis's acid-base constants obtained by Dai et al. [21] and Lee et al. [27] were determined by neglecting the temperature effect on the surface area of organic molecules, which is necessary to use for an accurate determination of the polar enthalpy and then the caid-base constants of materials. On the other hand, the approach of Lee et al. [27] used the deformation polarizability of molecules without taking into account that of the solid substrates. The correction made by our new methodology led to accurate determination of the Lewis's acid-base parameters of the different solid materials.

### *2.3. Polar Acid-Base Surface Energies of Graphenes and Carbon Fibers*

The polar acid $\gamma_s^+$ and base $\gamma_s^-$ surface energies of the different solid materials were determined by using the method of Van Oss et al. [87], knowing the values of polar free energy $-\Delta G_a^{sp}(T)$ of adsorbed solvents and their polar acid $\gamma_l^+$ and base $\gamma_l^-$ surface energies. The values of $-\Delta G_a^{sp}(T)$ were given in Table 6.

**Table 6.** Values of ($-\Delta G_a^{sp}(T)$ in kJ/mol) of dichloromethane and ethyl acetate adsorbed on solid materials at different temperatures.

| Dichloromethane | | | | | |
|---|---|---|---|---|---|
| T(K) | G | GO | rGO | UCF | OCF |
| 313.15 | 12.938 | 2.309 | 10.175 | 4.130 | 10.526 |
| 323.15 | 12.993 | 2.749 | 10.148 | 3.872 | 10.235 |
| 333.15 | 13.048 | 3.192 | 10.123 | 3.614 | 9.944 |
| 343.15 | 13.102 | 3.639 | 10.095 | 3.356 | 9.653 |
| 353.15 | 13.157 | 4.082 | 10.068 | 3.098 | 9.362 |
| 363.15 | 13.211 | 4.523 | 10.042 | 2.840 | 9.071 |
| 373.15 | 13.265 | 4.964 | 10.013 | 2.582 | 8.780 |
| Ethyl acetate | | | | | |
| T(K) | G | GO | rGO | UCF | OCF |
| 313.15 | 22.191 | 11.657 | 21.696 | 9.471 | 13.204 |
| 323.15 | 21.658 | 11.603 | 20.849 | 9.381 | 12.962 |
| 333.15 | 21.125 | 11.552 | 20.000 | 9.291 | 12.720 |
| 343.15 | 20.591 | 11.504 | 19.151 | 9.201 | 12.478 |
| 353.15 | 20.057 | 11.452 | 18.302 | 9.111 | 12.236 |
| 363.15 | 19.524 | 11.400 | 17.453 | 9.021 | 11.994 |
| 373.15 | 18.990 | 11.347 | 16.604 | 8.931 | 11.752 |

The values of the surface areas of polar solvents obtained using the Hamieh thermal model, and those of $-\Delta G_a^{sp}(T)$ in Table 6 led to the values of $\gamma_s^+$ and $\gamma_s^-$ of the different graphenes and carbon

 doi:10.20944/preprints202405.1631.v1



fibers and therefore to the polar acid-base surface energy $\gamma_s^p = 2\sqrt{\gamma_s^+\gamma_s^-}$. The total surface energy of the solid materials was obtained by summing the London dispersive and polar surface energy $\gamma_s^{tot.} = \gamma_s^d + \gamma_s^p$. The results given in Table S4 showed the highest values of the different components of surface energy of graphene respectively followed by those of oxidized carbon fiber, reduced graphene oxide, untreated carbon fibers, and graphene oxide. These results confirmed the highest values of $-\Delta G_a^{sp}(T)$ obtained for graphene surface.

The variations of polar acid-base energies $\gamma_s^+$, $\gamma_s^-$, $\gamma_s^p$, and total surface energy $\gamma_s^{tot.}$ of the different graphenes and carbon materials as a function of temperature, were plotted in Figure 7. It can be easily observed that graphene exhibited the highest values of the different components of surface energy, whereas reduced graphene oxide and oxidized carbon fibers exhibited close polar basic surface energy, while the lowest basic surface energy was obtained with graphene oxide and untreated carbon fibers. The results of the acidic surface energy showed the highest value for graphene followed by reduced graphene oxide whereas, the lowest values were observed respectively with oxidized carbon fibers, graphene oxide, and untreated carbon fibers. The same conclusions were observed in Figure 7 for the polar and total surface energy of materials.

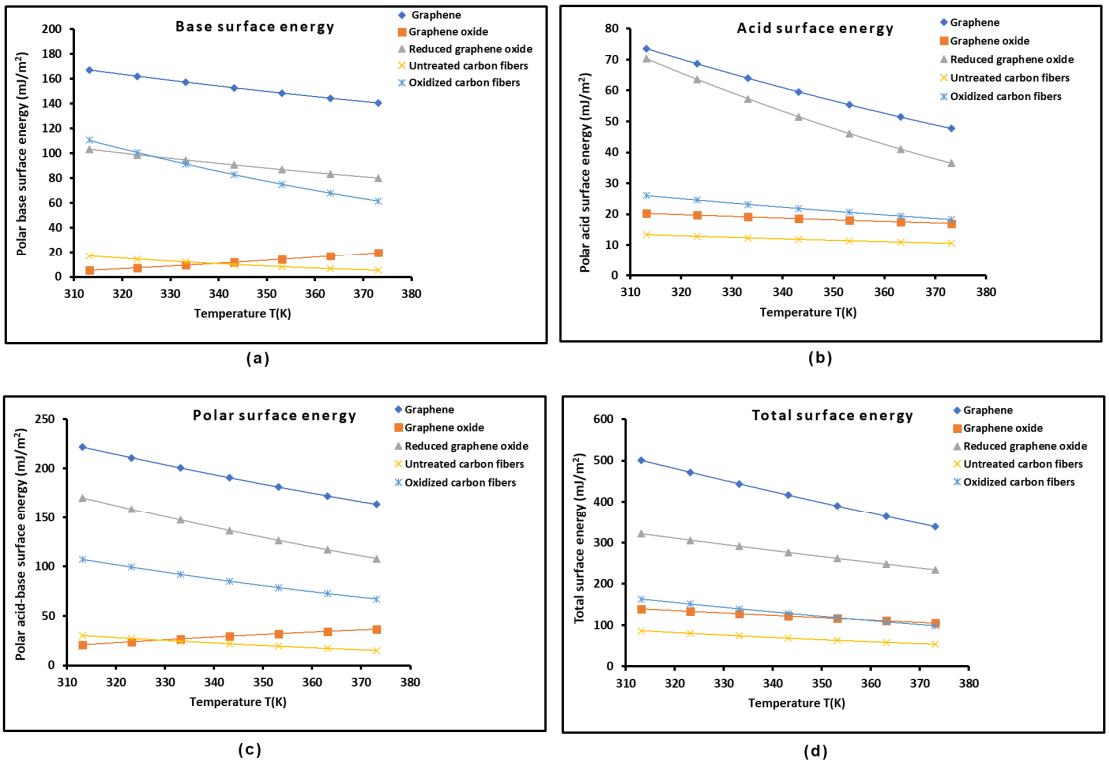


**Figure 7.** Evolution of polar acid-base energies $\gamma_s^-$ (a), $\gamma_s^+$ (b), $\gamma_s^p$ (c), and total surface energy $\gamma_s^{tot.}$ (d) (in mJ/m$^2$) of the different graphenes and carbon materials against temperature.

The previous results led to the values of polar surface energy of the different organic solvents using Fowkes relation [88] and the values of surface area of molecules obtained from the Hamieh thermal model as a function of temperature. Obtained results were given in curve forms in Figure 8 for the different polar organic molecules adsorbed on solid materials.

 doi:10.20944/preprints202405.1631.v1



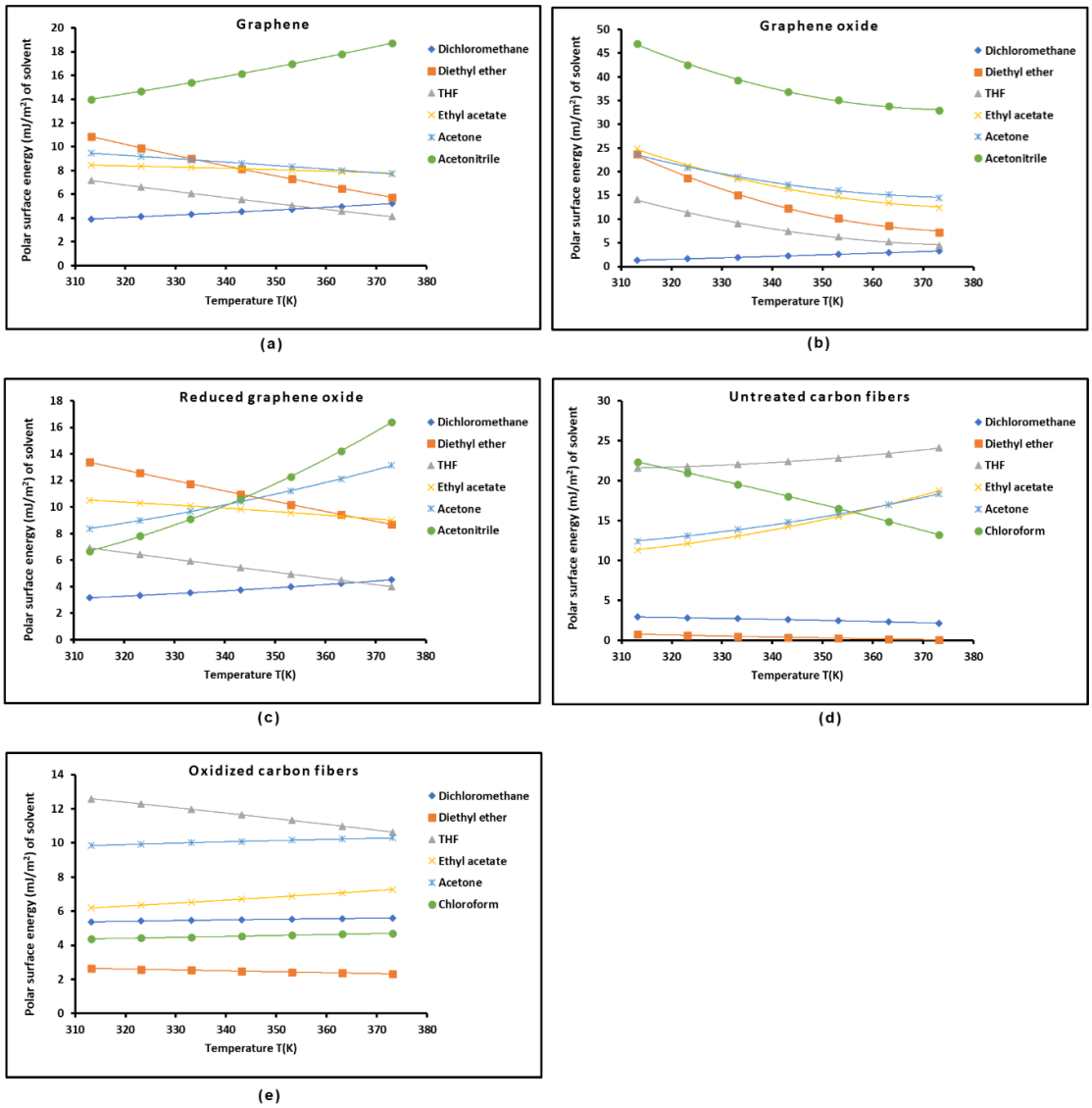


**Figure 8.** Variations of polar surface energy (in $mJ/m^2$) of different organic solvents adsorbed on Graphene (a), Graphene oxide (b), Reduced graphene oxide (c), Untreated carbon fibers (d), and Oxidized carbon fibers (e) as a function of temperature.

The polar surface energy of acetonitrile was shown in Figure 8 to be the highest for the three graphene surfaces. It was observed the polar energy of the different organic solvents were the highest in the case of graphene oxide and untreated carbon fiber. This result cannot be taken separately. To conclude, it is necessary to determine the adhesion work of the polar molecules adsorbed on solid surfaces. The different results given in this work can help experts to obtain interesting information on the adhesion work as a function of the temperature. Here, it can be mentioned that the new methodology proposed to quantify the surface properties of solid substrates using inverse gas chromatography will be very useful for readers interested in the determination of acid-base properties and surface energy of materials.

*2.4. Determination of the Average Separation Distance H*

The experimental results shown in Figure S1 and Table S1 led to the determination of the average separation distance $H$ between the solid graphenes and carbon fibers and the organic molecules as a function of the temperature, by using our new approach based on the London dispersion interaction.

 doi:10.20944/preprints202405.1631.v1



The results were given in Figure 9 which clearly showed an effect of the temperature on the average separation distance. An increase of the distance $H(T)$ versus the temperature was observed for all solid materials.

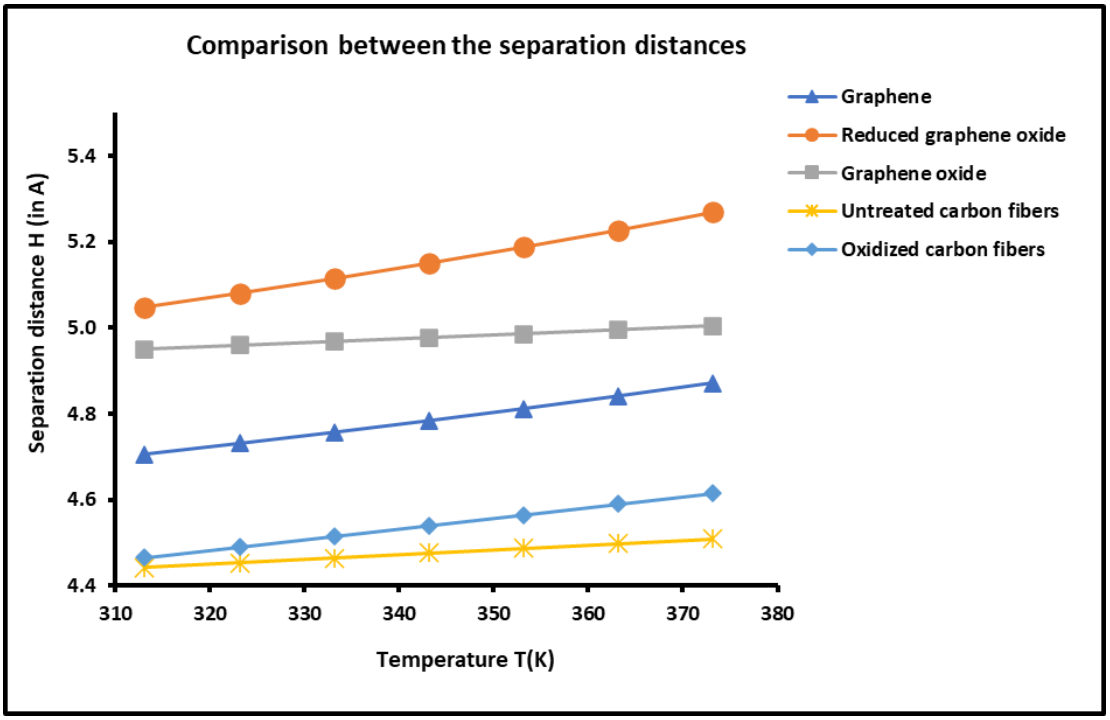


**Figure 9.** Variations of the average separation distance $\boldsymbol{H(T)}$ (in Å) between graphenes and carbon fibers, and organic molecules as a function of the temperature.

The thermal effect on the distance $H(T)$ shown in Figure 9 led to classify graphenes and carbon fibers in decreasing order of $H(T)$:

$$rGO > GO > G > OCF > UCF$$

This important result can be correlated to the interaction between materials and organic solvents. Indeed, when the attractive interaction force increases, the separation distance decreases. It seems that this result is in good agreement with those obtained with the Lewis acid-base properties. The above classification order of the distance $H$ is perfectly inversed in the Lewis base constant $K_D$ of graphenes and carbon fibers, which confirms that when the basicity of solid surface decreases, the distance with basic organic molecules increases.

### 3. Materials and Methods Thermal Model

All chemicals such organic molecules, carbon fibers, graphene G, graphene oxide OG, and reduced graphene rOG solid materials used in this study were purchased from Fisher Scientific (Beirut, Lebanon). The non-polar solvents such as pentane, hexane, heptane, octane, nonane, and decane were utilized to determine the London dispersive properties of the different solid substrates. The polar solvents were used to determine the polar parameters of interaction with the solid surfaces. The Lewis acid molecules were the following: carbon tetrachloride ($CCl_4$), chloroform ($CHCl_3$) and dichloromethane ($CH_2Cl_2$). The amphoteric solvents were acetone and acetonitrile, and the basic molecules were ethyl acetate, diethyl ether and tetrahydrofuran (THF). The two carbon fibers were previously analyzed: untreated fibers and oxidized fibers [74]. The corrected acceptor number and normalized donor number of the electrons of the polar solvents were given in other papers [74–76].

 doi:10.20944/preprints202405.1631.v1



Experimental measurements were performed on a commercial Focus GC gas chromatograph equipped with a flame ionization detector (Sigma-Aldrich, St. Quentin Fallavier, France). The solid particles were filled into a stainless-steel column with a 2 mm inner diameter and a length of 20 cm. The temperature range varied from 40 °C to 100 °C. The column was packed with 1 g of solid particles. The standard deviation of the obtained retention time, $t_R$, was less than 1% in all measurements. The temperatures of the injector and detector were fixed at 200 °C. The infinite dilution of the probes was satisfied by using 1 µL Hamilton syringes and injecting very small quantities of the vapor probe, satisfying the limit of detection of the FID of high sensitivity, to practically realize the zero-surface coverage [60,75]. The columns containing the solid particles were preconditioned at 130 °C overnight to insure the total desorption of water molecules or any other residual impurities [60,75].

The chromatographic experiments of net retention time $t_n$ of adsorbed molecules led to their net retention volume $V_n$. The free energy $\Delta G_a^0$ of adsorption of solvents on the solid materials is then obtained by the following equation:

$$\Delta G_a^0 = -RT\, lnV_n + B(T), \tag{1}$$

where $T$ is the absolute temperature, $R$ the perfect gas constant, and $B(T)$ is a constant depending on the temperature and the two-dimensional reference state of the adsorbed film.

The surface variable $\Delta G_a^0$ can be written as follows:

$$\Delta G_a^0 = \Delta G_a^d + \Delta G_a^p, \tag{2}$$

where $\Delta G_a^d$ and $\Delta G_a^p$ are respectively the London dispersion component and the polar component of the free energy adsorption.

Many methods or models were used in literature [40,68–70,72,73] to separate the London dispersive and polar contributions of the total free energy of interaction. However, these methods were proved in several recent studies that they cannot be used as quantitative due to some gaps, incoherencies, and irregularities in their concepts and applications. We proposed more rigorous method for the separation of the London dispersive and polar terms, based on the London dispersive interaction energy between the solvents and the solid surfaces [75,76].

The determination of the London dispersive component $\gamma_s^d$ of the surface energy of solid materials was also corrected by using the Hamieh thermal model [22–26] taking into account the temperature effect on the surface area of organic molecules and on the London dispersive component $\gamma_l^d$ of the surface energy of solvents.

The London dispersion free energy can be expressed as:

$$\Delta G_a^d(T) = -\frac{\alpha_{0S}}{H^6}\left[\frac{3\mathcal{N}}{2(4\pi\varepsilon_0)^2}\left(\frac{\varepsilon_S\,\varepsilon_X}{(\varepsilon_S+\varepsilon_X)}\alpha_{0X}\right)\right], \tag{3}$$

where $\mathcal{N}$ is the Avogadro's number, $\varepsilon_0$ is the permittivity of vacuum, $S$ denotes the solid particle, $X$ is the solvent molecule separated by a distance $H$, and $\varepsilon_S$ and $\varepsilon_X$ are the respective ionization energies of the solid $S$ and the solvent $X$. The new parameter of interaction taken for the quantification of the polar free energy of interaction is given by:

$$\mathcal{P}_{SX} = \frac{\varepsilon_S\,\varepsilon_X}{(\varepsilon_S+\varepsilon_X)}\alpha_{0X}. \tag{4}$$

For n-alkanes $(C_n)$ adsorbed on the solid material, the energetic parameter $RTlnVn(C_n)$ of adsorption is expressed by:

$$RTlnVn(C_n) = A\left[\frac{3\mathcal{N}}{2(4\pi\varepsilon_0)^2}\mathcal{P}_{SX}(C_n)\right] - B. \tag{5}$$

The constant $A$ is given by:

$$A = \frac{\alpha_{0S}}{H^6}. \tag{6}$$

The representation of $RTlnVn(C_n)$ against $\frac{3\mathcal{N}}{2(4\pi\varepsilon_0)^2}\mathcal{P}_{SX}(C_n)$ gave a straight-line of n-alkanes allowing the determination of the polar free energy $\left(-\Delta G_a^p(T)\right)$ of adsorbed polar solvents as a function of the temperature using the following equation:

 doi:10.20944/preprints202405.1631.v1



$$-\Delta G_a^p(T) = RTlnVn(X) - A\left[\frac{3\mathcal{N}}{2(4\pi\varepsilon_0)^2}\mathcal{P}_{S-X}\right] + B \quad (7)$$

This led to the polar enthalpy $-\Delta H_a^p(T)$ and entropy $-\Delta S_a^p(T)$ of organic molecules using the following thermodynamic relations:

$$\begin{cases} \Delta H_a^p(T) = \frac{\partial\left(\frac{\Delta G_a^p(T)}{T}\right)}{\partial\left(\frac{1}{T}\right)} \\ \Delta S_a^p(T) = -\left(\frac{\partial\left(\Delta G_a^p(T)\right)}{\partial T}\right) \end{cases} \quad (8)$$

The values of $-\Delta H_a^p(T)$ and $-\Delta S_a^p(T)$ of adsorbed polar solvents were obtained as a function of the temperature, and they allowed us to quantify This allowed obtaining the Lewis enthalpic acid–base constants $K_A$ and $K_D$ and the entropic acid–base parameters $\omega_A$ and $\omega_D$:

$$\begin{cases} -\Delta H^p = DN \times K_A + AN \times K_D \\ -\Delta S^p = DN \times \omega_A + AN \times \omega_D \end{cases} \quad (9)$$

where *AN* and *DN* are, respectively, the Gutmann electron donor and acceptor numbers of the polar solvents [89]. The used values were those corrected by Riddle and Fowkes [90].

The surface energy of solid surfaces can be written as:

$$\gamma_s = \gamma_s^d + \gamma_s^p \quad (10)$$

where $\gamma_s^p$ represents the total polar (or acid-base) contribution $\gamma_s^p$ of the surface energy.

The determination of $\gamma_s^d(T)$ of the various solid materials was determined using Fowkes relation [88] and the Hamieh thermal model giving the surface area $a(T)$ of organic molecules as a function of the temperature [22–26]:

$$RTlnV_n = 2\mathcal{N}a(T)\left(\gamma_l^d\gamma_s^d\right)^{1/2} + \alpha(T) \quad (11)$$

where $\alpha(T)$ is a constant depending only on the temperature and the solid material.

To determine $\gamma_s^p$ of the different solid surfaces, we applied Van Oss et al.'s method [87] that consists first in the determination of the Lewis acid $\gamma_s^+$ and base $\gamma_s^-$ surface energies of solids knowing the Lewis acid $\gamma_l^+$ and base $\gamma_l^-$ surface energies of the used solvents and therefore the value of $\gamma_s^p$ will be determined. To do that, two monopolar solvents, ethyl acetate (*B*) and dichloromethane (*A*), were used by Van Oss et al. [87]. They are characterized by:

$$\begin{cases} \gamma_A^+ = 5.2\ mJ/m^2\ , \gamma_A^- = 0 \\ \gamma_B^+ = 0\ , \gamma_B^- = 19.2\ mJ/m^2 \end{cases} \quad (12)$$

Knowing the polar-free energy $\Delta G_a^{sp}(T)$ of the polar molecules, Van Oss et al. proposed the following relation [87]:

$$\Delta G_a^p(T) = 2\mathcal{N}a(T)\left(\sqrt{\gamma_l^-\gamma_s^+} + \sqrt{\gamma_l^+\gamma_s^-}\right) \quad (13)$$

The Lewis acid and base surface energies of the solid surfaces are then given by:

$$\begin{cases} \gamma_s^+(\mathrm{T}) = \frac{\left[\Delta G_a^p(T)\,(B)\right]^2}{4\mathcal{N}^2[a_B(T)]^2\gamma_B^-} \\ \gamma_s^-(\mathrm{T}) = \frac{\left[\Delta G_a^p(T)\,(A)\right]^2}{4\mathcal{N}^2[a_A(T)]^2\gamma_A^+} \end{cases} \quad (14)$$

This led to the polar (or acid–base) surface energy $\gamma_s^p = \gamma_s^{AB}$ and the total surface energy $\gamma_s^{tot.}$ of different materials:

$$\begin{cases} \gamma_s^{AB} = 2\sqrt{\gamma_s^+\gamma_s^-} \\ \gamma_s^{tot.} = \gamma_s^d + \gamma_s^{AB} \end{cases} \quad (15)$$

## 4. Conclusions

 doi:10.20944/preprints202405.1631.v1



The application of our new approach consisting in the use of the London dispersion interaction, the Hamieh thermal model, and the model of coupling amphoteric constant, by inverse gas chromatography at infinite dilution, led to accurate determination of the surface properties of graphene, graphene oxide, reduced graphene oxide, untreated carbon fibers, and oxidized carbon fibers. Indeed, the London dispersion equation allowed the separation of the dispersive and polar contributions of the free energy of adsorption of organic molecules on graphenes and carbon materials, and consequently, led to the quantification of polar surface thermodynamic variables and acid-base constants of these materials. Whereas, the Hamieh thermal model conducted to a better determination of the London dispersive surface energy, the polar surface energy, the acid and base surface energy of solid surfaces as well as the polar surface energy of organic solvents adsorbed on graphenes and carbon fibers. Furthermore, the model of third amphoteric constant corrected the values of Lewis acid-base constants of solid materials. A successful first attempt consisting in correlating the thermal conductivity of graphenes and carbon fibers to their London dispersive surface energy. It was proved that graphene exhibiting the highest thermal conductivity, has also the highest London dispersive and polar surface energies. This new approach corrected some serious errors and deficiencies made in literature by some authors. This study gave for the first time the variations of polar surface energy of graphenes as well as the acid and base surface energy as a function of temperature. The various results obtained in this work all converge towards the final conclusion of the highest polar and dispersive characteristics of graphene and it highest Lewis's acid-base behavior.

**Supplementary Materials:** The following supporting information can be downloaded at the website of this paper posted on Preprints.org. Figure S1. Variations of $RTlnV_n(T)$ of n-alkanes and polar molecules adsorbed on the various solid materials against the temperature. (a): Graphene, (b): Graphene oxide, (c): Reduced graphene oxide, (d) Untreated carbon fibers, and (e): Oxidized carbon fibers. Table S1. Values of $-\Delta G_a^p(T)$ (in kJ/mol) of polar molecules adsorbed on the various solid materials against the temperature. Graphene, Graphene oxide, Reduced graphene oxide, Untreated carbon fibers, and Oxidized carbon fibers. Table S2. Values of ($-\Delta H_a^p$ in kJ $mol^{-1}$) of polar molecules adsorbed on the different graphene and carbon materials Table S3. Values of ($-\Delta S_a^p$ in J $K^{-1}mol^{-1}$) of polar molecules adsorbed on the different graphene and carbon materials Table S4. Values of polar acid-base energies $\gamma_s^+$, $\gamma_s^-$, $\gamma_s^p$, and total surface energy $\gamma_s^{tot.}$ (in $mJ/m^2$) of the different graphenes and carbon materials at various temperatures

**Funding:** This research received no external funding

**Informed Consent Statement:** Not applicable

**Data Availability Statement:** The data presented in this study are available in article and supplementary materials.

**Conflicts of Interest:** The author declares no conflicts of interest.

## References

1. Balandin, A. Thermal properties of graphene and nanostructured carbon materials. *Nature Mater* **10**, 569–581 (2011). https://doi.org/10.1038/nmat3064
2. Novoselov, K. S. et al. Electric field effect in atomically thin carbon films. *Science* **306,** 666–669 (2004).
3. Geim, A. K. & Novoselov, K. S. The rise of graphene. *Nature Mater*. **6,** 183–191 (2007).
4. Novoselov, K. S. et al. Two-dimensional gas of massless Dirac fermions in graphene. *Nature* **438,** 197–200 (2005).
5. Zhang, Y. B., Tan, Y. W., Stormer, H. L. & Kim, P. Experimental observation of the quantum Hall effect and Berry's phase in graphene. *Nature* **438,** 201–204 (2005).
6. Balandin, A.A.; Ghosh, S.; Bao, W.; Calizo, I.; Teweldebrhan, D.; Miao, F.; Lau, C.N. Superior thermal conductivity of single-layer graphene, *Nano Lett*., **2008**, *8*, 902-907, https://doi.org/10.1021/nl0731872.
7. Ghosh, S. et al. Extremely high thermal conductivity in graphene: Prospects for thermal management application in nanoelectronic circuits. *Appl. Phys. Lett*. **92,** 151911 (2008).
8. Calizo, I., Balandin, A. A., Bao, W., Miao, F. & Lau, C. N. Temperature dependence of the Raman spectra of graphene and graphene multilayers. *Nano Lett.* **7,** 2645–2649 (2007).

9. Ghosh, S. et al. Thermal properties of polycrystalline graphene films and reduced graphene-oxide films. *MRS Proc.* **S6.2,** 198 (2010).
10. Kole, M.; Dey, T.K. Investigation of thermal conductivity, viscosity, and electrical conductivity of graphene based nanofluids. *J. Appl. Phys.*, 2013, https://doi.org/10.1063/1.4793581.
11. Kumar, P.V.; Bardhan; N.M.; Tongay, S.; Wu, J.; Belcher, A.M.; Grossman, J.C. Scalable enhancement of graphene oxide properties by thermally driven phase transformation. Nat. Chem., **2014**, *6*, 151–158. doi:10.1038/nchem.1820.
12. Lee, J.W.; Ko, J.M.; Kim, J.-D. Hydrothermal preparation of nitrogen-doped graphene sheets via hexamethylenetetramine for application as supercapacitor electrodes. Electrochim Acta, **2012**, *85*, 459–466. doi:10.1016/j.electacta.2012.08.070.
13. Novoselov, K.; Fal'ko, V.; Colombo, L.; Gellert, P.R.; Schwab, M.G.; Kim, K. A roadmap for graphene. *Nature* **490**, 192–200 (2012). https://doi.org/10.1038/nature11458
14. Lopez Paz, I., Godignon, P., Moffat, N. et al. Position-resolved charge collection of silicon carbide detectors with an epitaxially-grown graphene layer. *Sci Rep* **14**, 10376 (2024). https://doi.org/10.1038/s41598-024-60535-3
15. Dai, J.; Wang, G.; Wu, C. Progress in Surface Properties and the Surface Testing of Graphene. *Journal of Advances in Physical Chemistry* **2016**, *05* (02), 48-57. https://doi.org/10.12677/JAPC.2016.52006
16. Amanda, S. B. & Ian, K. S. Thermal stability of graphene edge structure and graphene nanoflakes. *J. Chem. Phys.* **128**, 094707 (2008).
17. Xiong, Z., Yu, P., Liang, Q. et al. Rapid microwave reduction of electrochemically-derived graphene oxide for high-crystalline graphene membranes. *Sci. China Mater.* **66**, 4733–4741 (2023). https://doi.org/10.1007/s40843-023-2640-4
18. Liu, J., Li, Q. & Xu, S. Reinforcing mechanism of graphene and graphene oxide sheets on cement-based materials. *J. Mater. Civ. Eng*. **31**, 04019014 (2019).
19. Kumuda, S., Gandhi, U., Mangalanathan, U. et al. Synthesis and characterization of graphene oxide and reduced graphene oxide chemically reduced at different time duration. *J Mater Sci: Mater Electron* **35**, 637 (2024). https://doi.org/10.1007/s10854-024-12393-y
20. Shiren Wang, Yue Zhang, Noureddine Abidi, and Luis Cabrales, Wettability and Surface Free Energy of Graphene Films, *Langmuir* **2009**, *25* (18), 11078-11081, https://doi.org/10.1021/la901402f
21. Dai, J.; Wang, G.; Wu, C. Investigation of the Surface Properties of Graphene Oxide and Graphene by Inverse Gas Chromatography. *Chromatographia* **2014**, *77* (3-4), 299-307. https://doi.org/10.1007/s10337-013-2597-1
22. Hamieh, T. Study of the temperature effect on the surface area of model organic molecules, the dispersive surface energy and the surface properties of solids by inverse gas chromatography. *J. Chromatogr. A* **2020**, *1627*, 461372.
23. Hamieh, T.; Ahmad, A.A.; Roques-Carmes, T.; Toufaily, J. New approach to determine the surface and interface thermodynamic properties of H-β-zeolite/rhodium catalysts by inverse gas chromatography at infinite dilution. *Sci. Rep.* **2020**, *10*, 20894.
24. Hamieh, T. New methodology to study the dispersive component of the surface energy and acid–base properties of silica particles by inverse gas chromatography at infinite dilution. *J. Chromatogr. Sci.* **2022**, *60*, 126–142. https://doi.org/10.1093/chromsci/bmab066.
25. Hamieh, T. Some Irregularities in the Evaluation of Surface Parameters of Solid Materials by Inverse Gas Chromatography. *Langmuir* **2023, *39*, 17059–17070**. https://doi.org/10.1021/acs.langmuir.3c01649.
26. Hamieh, T. Inverse Gas Chromatography to Characterize the Surface Properties of Solid Materials. *Chem. Mater.* **2024**, *36*, 5, 2231–2244. https://doi.org/10.1021/acs.chemmater.3c03091.
27. Lee, S.-Y.; Lee, J.-H.; Kim, Y-H.; Mahajan, R. L.; Park, S.-J. Surface energetics of graphene oxide and reduced graphene oxide determined by inverse gas chromatographic technique at infinite dilution at room temperature, *Journal of Colloid and Interface Science*, 2022, 628, 758-768, https://doi.org/10.1016/j.jcis.2022.07.183
28. Papadopoulou, S.K.; Panayiotou, C. Assessment of the thermodynamic properties of poly(2,2,2-trifluoroethyl methacrylate) by inverse gas chromatography. *J. Chromatogr. A* **2014**, 1324, 207–214.
29. Voelkel, A.; Strzemiecka, B.; Adamska, K.; Milczewska, K. Inverse gas chromatography as a source of physiochemical data. *J. Chromatogr. A* **2009**, *1216*, 1551.
30. Al-Saigh, Z.Y.; Munk, P. Study of polymer-polymer interaction coefficients in polymer blends using inverse gas chromatography, *Macromolecules* **1984**, *17*, 803.
31. Dritsas, G.S.; Karatasos, K.; Panayiotou, C. Investigation of thermodynamic properties of hyperbranched aliphatic polyesters by inverse gas chromatography, *J. Chromatogr. A* **2009**, *1216*, 8979.
32. Papadopoulou, S.K.; Panayiotou, C. Thermodynamic characterization of poly(1,1,1,3,3,3-hexafluoroisopropyl methacrylate) by inverse gas chromatography. *J. Chromatogr. A* **2012**, *1229*, 230.

 doi:10.20944/preprints202405.1631.v1




33. Coimbra, P.; Coelho, M. S.N.; Gamelas, J. A.F. Surface characterization of polysaccharide scaffolds by inverse gas chromatography regarding application in tissue engineering, *Surface and Interface Analysis*, 2019, 51 (11), 1070 – 1077.
34. Kołodziejek, J.; Voelkel, A.; Heberger, K. Characterization of hybrid materials by means of inverse gas chromatography and chemometrics. *J. Pharm. Sci*. **2013**, *102*, 1524.
35. Belgacem, M.N.; Czeremuszkin, G.; Sapieha, S.; Gandini, A. Surface by XPS characterization and inverse gas of cellulose fibres chromatography. *Cellulose* **1995**, *2*, 145–157.
36. Ryan, H.M.; Douglas, J.G.; Rupert, W. Inverse Gas Chromatography for Determining the Dispersive Surface Free Energy and Acid–Base Interactions of Sheet Molding Compound-Part II 14 Ligno-Cellulosic Fiber Types for Possible Composite Reinforcement. *J. Appl. Polym. Sci.* **2008**, *110*, 3880–3888.
37. Jacob, P.N.; Berg, J.C. Acid-base surface energy characterization of microcrystalline cellulose and two wood pulp fiber types using inverse gas chromatography. *Langmuir* **1994**, *10*, 3086–3093.
38. Carvalho, M.G.; Santos, J.M.R.C.A.; Martins, A.A.; Figueiredo, M.M. The Effects of Beating, Web Forming and Sizing on the Surface Energy of *Eucalyptus globulus* Kraft Fibres Evaluated by Inverse Gas Chromatography. *Cellulose* **2005**, *12*, 371–383.
39. Chtourou, H.; Riedl, B.; Kokta, B.V. Surface characterizations of modified polyethylene pulp and wood pulps fibers using XPS and inverse gas chromatography. *J. Adhesion Sci. Tech*. **1995**, *9*, 551–574.
40. Donnet, J.B.; Park, S.J.; Balard, H. Evaluation of specific interactions of solid surfaces by inverse gas chromatography. *Chromatographia* **1991**, *31*, 434–440.
41. Donnet, J.B.; Custodéro, E.; Wang, T.K.; Hennebert, G. Energy site distribution of carbon black surfaces by inverse gas chromatography at finite concentration conditions. *Carbon* **2002**, *40*, 163–167. https://doi.org/10.1016/S0008-6223(01)00168-3.
42. Gamble, J.F.; Davé, R.N.; Kiang, S.; Leane, M.M.; Tobyn, M.; Wang, S.S.Y. Investigating the applicability of inverse gas chromatography to binary powdered systems: An application of surface heterogeneity profiles to understanding preferential probe-surface interactions. *Int. J. Pharm.* **2013**, *445*, 39–46.
43. Balard, H.; Maafa, D.; Santini, A.; Donnet, J.B. Study by inverse gas chromatography of the surface properties of milled graphites. *J. Chromatogr. A* **2008,** *1198–1199*, 173–180.
44. Bogillo, V.I.; Shkilev, V.P.; Voelkel, A. Determination of surface free energy components for heterogeneous solids by means of inverse gas chromatography at finite concentrations. *J. Mater. Chem.* **1998**, *8*, 1953–1961.
45. Das, S.C.; Zhou, Q.; Morton, D.A.V.; Larson, I.; Stewart, P.J. Use of surface energy distributions by inverse gas chromatography to understand mechanofusion processing and functionality of lactose coated with magnesium stearate. *Eur. J. Pharm. Sci*. **2011**, *43*, 325–333.
46. Das, S.C.; Stewart, P.J. Characterising surface energy of pharmaceutical powders by inverse gas chromatography at finite dilution. *J. Pharm. Pharmacol*. **2012**, *64*, 1337–1348.
47. Bai, W.; Pakdel, E.; Li, Q.; Wang, J.; Tang, W.; Tang, B.**;** Wang, X. Inverse gas chromatography (IGC) for studying the cellulosic materials surface characteristics: a mini review, *Cellulose,* **2023**, 30, 3379–3396, https://doi.org/10.1007/s10570-023-05116-9.
48. Dong, S.; Brendlé, M.; Donnet, J.B. Study of solid surface polarity by inverse gas chromatography at infinite dilution. *Chromatographia* **1989**, *28*, 469–472.
49. Gamble, J.F.; Leane, M.; Olusanmi, D.; Tobyn, M.; Supuk, E.; Khoo, J.; Naderi, M. Surface energy analysis as a tool to probe the surface energy characteristics of micronized materials—A comparison with inverse gas chromatography. *Int. J. Pharm.* **2012**, *422*, 238–244.
50. Newell, H.E.; Buckton, G.; Butler, D.A.; Thielmann, F.; Williams, D.R. The use of inverse gas chromatography to measure the surface energy of crystalline, amorphous, and recently milled lactose. *Pharm. Res*. **2001**, *18*, 662–666.
51. Newell, H.E.; Buckton, G. Inverse gas chromatography: Investigating whether the technique preferentially probes high energy sites for mixtures of crystalline and amorphous lactose. *Pharm. Res.* **2004**, *21*, 1440–1444.
52. Kołodziejek, J.; Głowka, E.; Hyla, K.; Voelkel, A.; Lulek, J.; Milczewska, K. Relationship between surface properties determined by inverse gas chromatography and ibuprofen release from hybrid materials based on fumed silica. *Int. J. Pharm.* **2013**, *441*, 441–448.
53. Ho, R.; Hinder, S.J.; Watts, J.F.; Dilworth, S.E.; Williams, D.R.; Heng, J.Y.Y. Determination of surface heterogeneity of D-mannitol by sessile drop contact angle and finite concentration inverse gas chromatography. *Int. J. Pharm*. **2010**, *387*, 79–86.
54. Sesigur, F.; Sakar, D.; Yazici, O.; Cakar, F.; Cankurtaran, O.; Karaman, F. Dispersive Surface Energy and Acid-Base Parameters of Tosylate Functionalized Poly(ethylene glycol) via Inverse Gas Chromatography. *J. Chem.* **2014**, *2014*, 402325.
55. Calvet, R.; Del Confetto, S.; Balard, H.; Brendlé, E.; Donnet, J.B. Study of the interaction polybutadiene/fillers using inverse gas chromatography. *J. Chromatogr. A* **2012**, *1253*, 164–170.
56. Papadopoulou, S.K.; Dritsas, G.; Karapanagiotis, I.; Zuburtikudis, I.; Panayiotou, C. Surface characterization of poly(2,2,3,3,3-pentafluoropropyl methacrylate) by inverse gas chromatography and contact angle measurements *Eur. Polym. J.* **2010**, *46*, 202–208.

57. Dritsas, G.S.; Karatasos, K.; Panayiotou, C. Investigation of thermodynamic properties of hyperbranched poly(ester amide) by inverse gas chromatography. *J. Polym. Sci. Polym. Phys.* **2008**, *46*, 2166–2172.
58. Hamieh, T.; Rezzaki, M.; Schultz, J. Study of the transition temperatures and acid–base properties of poly (methyl methacrylate) adsorbed on alumina and silica, by using inverse gas chromatography technique. *Colloids Surf. A Physicochem. Eng. Asp.* **2001**, *189*, 279–291. https://doi.org/10.1016/S0927-7757(01)00597-0.
59. Hamieh, T.; Schultz, J. New approach to characterise physicochemical properties of solid substrates by inverse gas chromatography at infinite dilution. I. II. And III. *J. Chromatogr. A* **2002**, *969*, 17–47. https://doi.org/10.1016/S0021-9673(02)00368-0.
60. Hamieh, T. Temperature Dependence of the Polar and Lewis Acid–Base Properties of Poly Methyl Methacrylate Adsorbed on Silica via Inverse Gas Chromatography. *Molecules* **2024**, *29*, 1688. https://doi.org/10.3390/molecules29081688.
61. Papirer, E.; Brendlé, E.; Ozil, F.; Balard, H. Comparison of the surface properties of graphite, carbon black and fullerene samples, measured by inverse gas chromatography. *Carbon* **1999**, *37*, 1265–1274. https://doi.org/10.1016/S0008-6223(98)00323-6.
62. Chung, D.L. *Carbon Fiber Composites*; Butterworth-Heinemann: Boston, MA, USA, 1994; pp. 3–65. https://doi.org/10.1016/C2009-0-26078-8.
63. Donnet, J.B.; Bansal, R.C. *Carbon Fibers*, 2nd ed.; Marcel Dekker: New York, NY, USA, 1990; 584p. https://doi.org/10.1201/9781482285390.
64. Hamieh, T. Surface acid-base properties of carbon fibres. *Adv. Powder Technol.* **1997**, *8*, 279–289.
65. Liu, Y.; Gu, Y.; Wang, S.; Li, M. Optimization for testing conditions of inverse gas chromatography and surface energies of various carbon fiber bundles. *Carbon Lett.* **2023**, *33*, 909–920. https://doi.org/10.1007/s42823-023-00472-9.
66. Pal, A.; Kondor, A.; Mitra, S.; Thua, K.; Harish, S.; Saha, B.B. On surface energy and acid–base properties of highly porous parent and surface treated activated carbons using inverse gas chromatography. *J. Ind. Eng. Chem.* **2019**, *69*, 432–443. https://doi.org/10.1016/j.jiec.2018.09.046.
67. Hamieh, T. New Physicochemical Methodology for the Determination of the Surface Thermodynamic Properties of Solid Particles. *AppliedChem* **2023**, *3*, 229–255. https://doi.org/10.3390/appliedchem3020015.
68. Sawyer, D.T.; Brookman, D.J. Thermodynamically based gas chromatographic retention index for organic molecules using salt-modified aluminas and porous silica beads. *Anal. Chem.* **1968**, *40*, 1847–1850. https://doi.org/10.1021/ac60268a015.
69. Saint-Flour, C.; Papirer, E. Gas-solid chromatography. A method of measuring surface free energy characteristics of short carbon fibers. 1. Through adsorption isotherms. *Ind. Eng. Chem. Prod. Res. Dev.* **1982**, *21*, 337–341. https://doi.org/10.1021/i300006a029.
70. Saint-Flour, C.; Papirer, E. Gas-solid chromatography: Method of measuring surface free energy characteristics of short fibers. 2. Through retention volumes measured near zero surface coverage. *Ind. Eng. Chem. Prod. Res. Dev.* **1982**, *21*, 666–669. https://doi.org/10.1021/i300008a031.
71. Basivi, *P.K.;* Hamieh, *T.;* Kakani, *V.;* Pasupuleti, *V.R.;* Sasikala, *G.;* Heo, *S.M.;* Pasupuleti, *K.S.;* Kim, *M.-D.;* Munagapati, *V.S.;* Kumar, *N.S.;* Wen, *J.-H.;* Kim, *C.W.* Exploring advanced materials: Harnessing the synergy of inverse gas chromatography and artificial vision intelligence, TrAC Trends in Analytical Chemistry, *2024, 173, 117655,* https://doi.org/10.1016/j.trac.2024.117655.
72. Brendlé, E.; Papirer, E. A new topological index for molecular probes used in inverse gas chromatography for the surface nanorugosity evaluation, 2. Application for the Evaluation of the Solid Surface Specific Interaction Potential. *J. Colloid Interface Sci.* **1997**, *194*, 217–224.
73. Brendlé, E.; Papirer, E. A new topological index for molecular probes used in inverse gas chromatography for the surface nanorugosity evaluation, 1. Method of Evaluation. *J. Colloid Interface Sci.* **1997**, *194*, 207–216.
74. Hamieh, T. The Effect of Temperature on the Surface Energetic Properties of Carbon Fibers Using Inverse Gas Chromatography. *Crystals* **2024**, *14*, 28. https://doi.org/10.3390/cryst14010028.
75. Hamieh, T. New Progress on London Dispersive Energy, Polar Surface Interactions, and Lewis's Acid–Base Properties of Solid Surfaces. *Molecules* **2024**, *29*, 949. https://doi.org/10.3390/molecules29050949.
76. Hamieh, T. London Dispersive and Lewis Acid-Base Surface Energy of 2D Single-Crystalline and Polycrystalline Covalent Organic Frameworks. *Crystals* **2024**, *14*, 148. https://doi.org/10.3390/cryst14020148.
77. Dai, J.; Wang, G; Ma, L., Wu C. Study on the surface energies and dispersibility of graphene oxide and its derivatives, J. Mater. Sci., 2015, 50, 3895–3907, DOI 10.1007/s10853-015-8934-z
78. Baoqin Fu. Surface Energy of Diamond Cubic Crystals and Anisotropy Analysis Revealed by Empirical Electron Surface Models. *Advances in Materials*, **2019**, *8* (2), 61-69. https://doi.org/10.11648/j.am.20190802.14
79. Frank J. Z.; Hermenzo D. J. Surface energy and the size of diamond crystals**,** *AIP Conf. Proc.*, **1996**, *370*, 163–166, https://doi.org/10.1063/1.50738
80. Zhang, J.-M.; Li, H.-Y.; Xu, K.-W. Ji, V. Calculation of surface energy and simulation of reconstruction for diamond cubic crystals (001) surface, *Applied Surface Science*, **2008**, *254* (13), 4128-4133, https://doi.org/10.1016/j.apsusc.2007.12.049.

 doi:10.20944/preprints202405.1631.v1




81. Jang, D.; Lee, S. Correlating thermal conductivity of carbon fibers with mechanical and structural properties, *Journal of Industrial and Engineering Chemistry*, **2020**, *89*, 115-118, https://doi.org/10.1016/j.jiec.2020.06.026.
82. Kim, S.K. ; Bae, H.S.; Yu, J.; Kim S.Y. Thermal conductivity of polymer composites with the geometrical characteristics of graphene nanoplatelets. *Sci. Rep*., **2016**, *6*, 26825, https://doi.org/10.1038/srep26825
83. Mahdavi, M.; Yousefi, E.; Baniassadi, M.; Karimpour, M.; Baghani M. Effective thermal and mechanical properties of short carbon fiber/natural rubber composites as a function of mechanical loading, *Appl. Therm. Eng*., **2017**, *117*, 8-16
84. Hadadian, M.; Goharshadi, E.K.; Youssefi, A. Electrical conductivity, thermal conductivity, and rheological properties of graphene oxide-based nanofluids, *J. Nanopart. Res*., **2014**, *16*, 2788. https://doi.org/10.1007/s11051-014-2788-1
85. Hofmeister, A.M. Thermal diffusivity and thermal conductivity of single-crystal MgO and $Al_2O_3$ and related compounds as a function of temperature. *Phys Chem Minerals*, **2014**, *41*, 361–371, https://doi.org/10.1007/s00269-014-0655-3
86. Wu, X.; Lee, J.; Varshney, V.; Wohlwend, J.L.; Roy, AK.; Luo, T. Thermal Conductivity of Wurtzite Zinc-Oxide from First-Principles Lattice Dynamics – a Comparative Study with Gallium Nitride. *Sci Rep*, **2016**, *6*, 22504 (2016). https://doi.org/10.1038/srep22504
87. Van Oss, C.J.; Good, R.J.; Chaudhury, M.K. Additive and nonadditive surface tension components and the interpretation of contact angles. *Langmuir* **1988**, *4*, 884. https://doi.org/10.1021/la00082a018
88. Fowkes, F.M. Surface and Interfacial Aspects of Biomedical Polymers; Andrade, J.D., Ed.; Plenum Press: New York, NY, USA, 1985; Volume I, pp. 337–372.
89. Gutmann, V. The Donor-acceptor Approach to Molecular Interactions; Plenum: New York, NY, USA, 1978
90. Riddle, F.L.; Fowkes, F.M. Spectral shifts in acid-base chemistry. Van der Waals contributions to acceptor numbers, Spectral shifts in acid-base chemistry. 1. van der Waals contributions to acceptor numbers. *J. Am. Chem. Soc*. **1990**, 112, 3259–3264. https://doi.org/10.1021/ja00165a001